

LATEST DEVELOPMENTS FOR PHOTOINJECTOR, SEEDING AND THz LASER SYSTEMS

C.P. Hauri^{1,2}, A. Trisorio¹, C. Vicario¹, C. Ruchert¹, ¹PSI, Switzerland
²Ecole Polytechnique Federale de Lausanne, Switzerland.

Abstract

We report the status of the laser system developments taking place at the Paul Scherrer Institute for the future hard x-ray SASE FEL (SwissFEL). Novel schemes for improving the electron gun drive laser's temporal and spatial shape are discussed as well as efforts towards a wavelength-tunable seed laser based on high-order harmonic generation (HHG). Finally first results on a laser-driven THz source are presented which provides high power single-cycle electric field transients at a central frequency around 1 THz.

INTRODUCTION

In compact hard x-ray FELs, the electron beam emittance is one of the key parameters for a high lasing performance. To ensure small emittance in laser-driven electron guns a flat top and homogeneous laser profile both in space and time is favorable. The generation of well-shaped picosecond (ps) pulses at high energy is however still challenging in the 250-300 nm spectral range since other requirements, such as high pulse energy stability, low arrival time jitter at the gun and high pointing stability needs to be provided equally. A direct transfer of well-established near-IR pulse shaping techniques [1] to the deep UV spectral region has turned out to be difficult and appropriate techniques for direct amplitude and phase shaping in the deep-UV are needed to fulfill the stringent requirements of modern compact FEL facilities. In this paper we describe the performance of the gun laser system currently used to commission the SwissFEL test injector at PSI [2]. We present our latest achievements on deep-UV pulse temporal shaping based on chirp-matched sum frequency generation (CM SFG). Transverse beam homogenization based on a conical capillary filter technique is also discussed. Finally we present first steps towards secondary light sources at SwissFEL such as high-power single cycle THz transients and soft x-ray radiation for seeding based on high-order harmonic generation (HHG).

LASER SYSTEM

The schematic of our Ti:Sa CPA system is shown in Fig. 1 (adapted from ref [2]). The oscillator delivers ultra-broadband pulses at 83 MHz and is used as seed for the 100 Hz booster amplifier which increases the pulses energy to 1μJ. After pre-amplification, the pulses are stretched to 500 ps in a double-pass Offner triplet and sent through an AOPDF (DAZZLER™ HR800 – Fastlite). The AOPDF allows the user to easily define the spectral amplitude filter prior to regenerative amplification and is furthermore used for optimal pulse compression by

higher-order phase compensation via phase-error feedback from an online SPIDER measurement. The core device of our amplifier is the regenerative amplifier (RA) with an intracavity Brewster-cut AOPGCF (MAZZLER™ – Fastlite) [3]. It provides ultra-wide-band amplification (up to 130 nm full width) with pulse energies of 0.4 mJ. The AOPGCF is a computer controlled programmable gain filter which allows gain narrowing compensation. This is done via a computer-based feedback optimization loop based on an error signal derived from the amplified output spectrum (recorded after the compressor) and a user-defined reference. The AOPGCF introduces spectral losses through partial diffraction of spectral components taking into account the gain shaping effects from all amplifier stages and all optical elements like mirrors, polarizers, gratings and waveplates. Both booster and RA are pumped with one diode-pumped solid-state frequency doubled Nd:YAG unit (Centurion-Quantel, 20 mJ @ 100 Hz). After the last two multipass amplifiers (MA) a pulse energy of 27 mJ is reached. A set of 6 Centurion lasers are used to pump the two power amplifiers. Multiplexing several pump lasers with 20 mJ instead of just one 120 mJ device is motivated by energy stability issue. In the scheme showed in Fig.1 all the optics and optical sub-systems, such as stretcher,

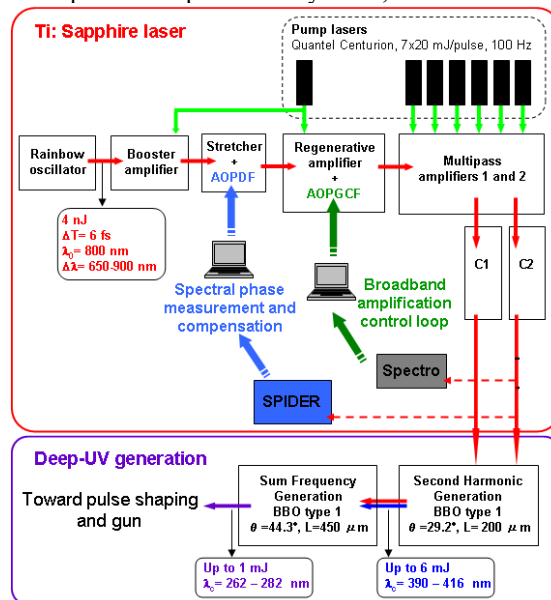


Figure 1: Schematic layout of the laser system with subsequent UV and deep-UV generation stage (adapted from [5]). AOPDF: acousto-optic programmable dispersive filter; AOPGCF: acousto-optic programmable gain control filter, C1: compressor 1 used for standard SFG setup, C2: compressor 2: used in parallel with compressor 1 for chirp-matched SFG.

amplifiers and the grating-based compressor support a maximum spectral bandwidth of 130 nm. This allows the generation of ultrashort pulses. On the other hand it is also possible to reduce the amplified spectrum down to 20 nm (FWHM). Temporal characterization of the amplified pulses is performed with a commercial diagnostic (Grenouille, Swamp optics) and the measured residual spectral phase is compensated with the AOPDF by feedback loop. Thanks to the spectral control the system can deliver transform limited pulses of 15 fs to 100 fs. The amplified pulse energy after compression is 20 mJ with a typical stability of 0.54 % RMS (4.4% P-P) over 5 minutes.

For daily electron gun operation, a pulse duration of 55 fs turned out to be best suited for high-energy second and third-harmonic frequency generation performed in β -barium borate (BBO) crystals. The third harmonic frequency is generated by sum frequency generation (SFG) of the fundamental and the second harmonic. In our standard configuration SFG is driven via compressor 1 (C1) output (see Fig. 1 for details). An additional compressor (C2) is available and used for the CM SFG experiment described below. The unique architecture of the Ti:Sa laser system offers wavelength tunability for narrow bandwidth pulses in the near IR (Fig. 2), as well as in the UV (after SHG) and the deep-UV (after SFG) spectral region (Fig. 3) The pulse energy measured in the deep-UV is up to 1 mJ with a stability of 0.7% RMS (5.6% P-P).

WAVELENGTH-TUNABLE SEED LASER

Such a high-power wavelength-tunable TW-class laser is beneficial for our future seeding applications with high-order harmonic (HH) radiation. The natural process of HHG provides a comb of odd harmonics up to the cut-off region. For optimal seeding of an FEL the frequency of the HH should exactly match the resonance frequency of the undulator. Tuning the HH is possible by tuning the fundamental laser frequency.

In principle, the 100 nm tuning range of our amplifier system provides a complete access to the wavelength range below 54 nm (Fig. 4) since neighboring harmonics starts to overlap for a fundamental laser tuned to the two extreme spectral positions (e.g. 750 nm and 850 nm). For HHG with a two-color laser (i.e. $\omega+2\omega$) an overlap of HH occurs already below 100 nm. In the latter case the harmonic content is doubled, since odd and even order HH are generated. Thus exact matching of the HH frequency to the undulator resonance frequency becomes feasible.

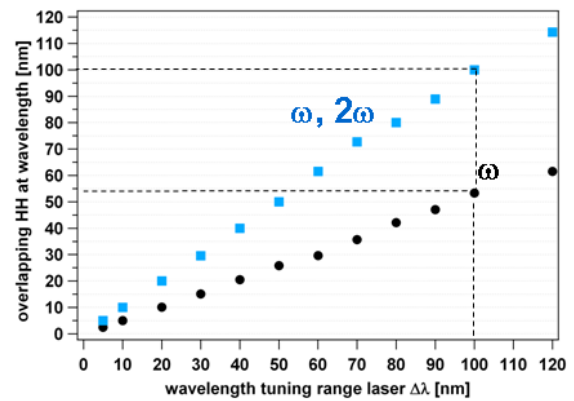


Figure 4: Wavelength-tuning range $\Delta\lambda$ required for fundamental laser to provide overlapping HH radiation.

CHIRPED MATCHED SFG

In this section, we present experiments where CM SFG [4] is used to generate high-energy ps flat top temporal profile in the deep-UV. CM SFG is based on tailoring the chirp of the two involved stretched ps pulses (fundamental and second harmonic) so that at any time the two instantaneous input frequencies produce a perfectly phase matched sum frequency in the deep UV. Because of the temporal walk-off, the condition cannot be exactly met through the entire crystal, but, if the temporal rate of chirp is small, the frequency change within the temporal walk-off will be negligible. In this case the spectral width is not restricted to the acceptance bandwidth of the crystal anymore, so much thicker crystals can be used which results in a significant increase of conversion efficiency while keeping the large conversion bandwidth attributed to thin crystals. For type 1 phase matching in BBO, the first order CM condition is satisfied for the SFG process $800+400 \rightarrow 266$ nm when the linear chirp parameters of the fundamental, Φ_1'' , and of the second harmonic Φ_2'' satisfy $\Phi_1''/\Phi_2'' = -1.8$ [5]. When the chirps are adjusted to match the above condition, one cannot simultaneously get full temporal overlap of the pulses, but for the parts that do overlap the spectral phase and intensity of the output pulse are simply related to the corresponding properties of the input pulses. In particular a strong coupling of fundamental spectral shape and deep UV temporal shape is present. Therefore, spectral IR shapers can be employed for high-resolution control of the temporal intensity profile in the deep-UV. This represents a new approach for the generation of temporally shaped pulses in the deep UV.

Figure 5 shows the experimental setup. For this experiment the amplifier the fundamental spectrum is chosen as $\lambda_0=800$ nm and $\Delta\lambda=30$ nm FWHM. A replica of the amplified pulse is split off after the last amplifier stage and separately compressed in an additional compressor. This way the two output pulses can be independently chirped and delayed to match the CM condition. The energy is unequally divided into the two beams (8 mJ and 5.7 mJ, respectively) to provide more energy for the SHG. The energy stability over 500 shots is

0.4 % rms and 2.7% ptp. Both the SHG and SFG stages are realized by BBO with type 11 phase matching. The SHG, which does not take advantage of the chirp matching, requires a thin crystal (0.1 or 0.2 mm) to support the necessary bandwidth. For the SFG a longer crystal, 0.8 mm, is used. The input IR pulse length is retrieved with a commercial auto-correlator (PulseCheck, APE GmbH). The output pulse at 267 nm is measured by cross-correlation with the same instrument. The residual IR pulse from the SHG is recompressed and used as probe (160 fs FWHM).

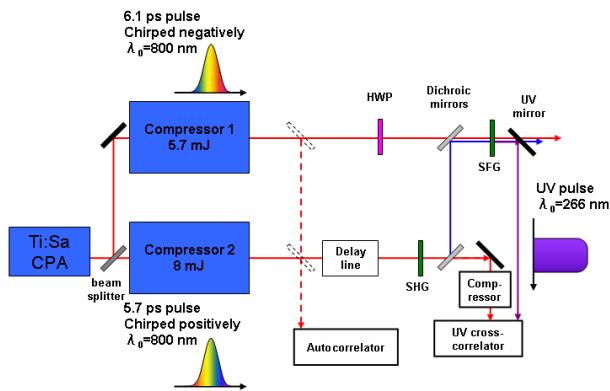


Figure 5: Experimental setup for chirped-matched sum frequency generation with picosecond pulses. The scheme allows direct generation of flattop-like picosecond pulses. (adapted from ref [6])

With this scheme both efficient SFG conversion and temporal pulse shaping in the picosecond regime becomes feasible. In CM case the SFG pulse becomes linearly chirped with temporal chirp rate equal to the sum of the ones of the input pulses. When stretching the fundamental beams to picoseconds the dispersion of the SFG crystal as well as higher order chirp can be neglected. In this configuration the temporal shape of the ps pulse is similar to its spectral shape. Since our application does not require transform limited pulses, we can take advantage of this fact and produce a top hat temporal deep-UV pulse by shaping the IR spectrum. The IR Dazzler is programmed to produce square-like IR spectrum extending over 30 nm with sharp edge of less than 2 nm (10-90% of the maximum intensity). The IR pulse length measured with the auto-correlator was 6.1 ps. The second IR pulse used for second harmonic generation was 5.7 ps long. The chirp of the fundamental and second harmonic were measured to be $-7.5 \cdot 10^4 \text{ fs}^2$ and $+4.05 \cdot 10^4 \text{ fs}^2$, respectively. For the SHG and the SFG, 0.1 mm and 0.8 mm BBO crystals were used. The resulting SFG spectrum is shown in Fig. 6. The deep UV spectrum has sharp edges, a flat top shape, and a full bandwidth of 2.5 nm. As comparison, the typical spectrum obtained with fs SFG is depicted in red dashed line. Due to the linear chirp the resulting temporal profile measured with crosscorrelator is also flat top (Fig. 6b). The pulse duration is 4.5 ps FWHM, rise and fall time are shorter than 0.7 ps and the modulation at the plateau are 10% rms and 39% P-P. Fine

adjustments of the relative delay between ω and 2ω is used to optimize the top hat pulse formation. The presented flattop ps pulses will be used for electron beam generation in the SwissFEL test injector facility in near future. The pulse energy of 220 uJ permits the generation of sufficient charge for standard metal photocathodes.

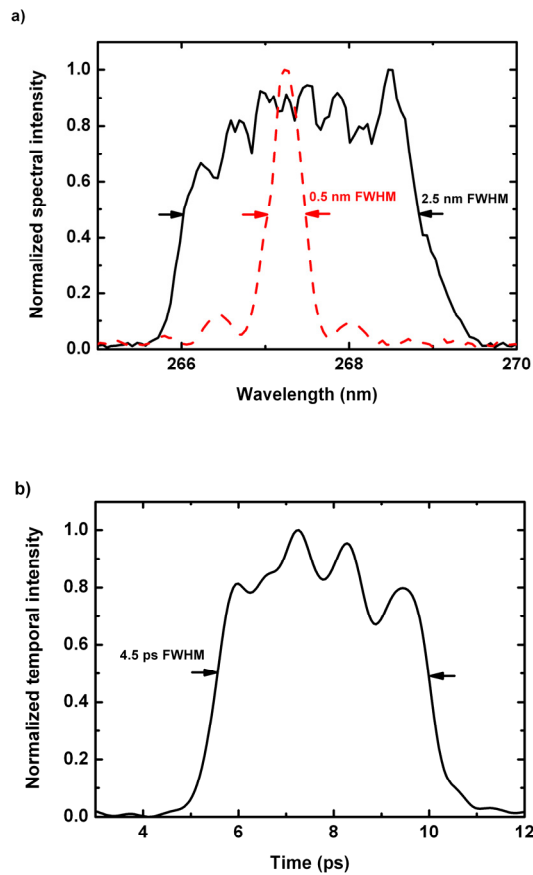


Figure 6: measured spectrum (a) and temporal profile (b) of the broadband flat-top pulse (black). As a comparison, the typical spectrum generated with fs SFG is shown (red dashed). (from ref[6])

SPATIAL BEAM SHAPING

Experience shows that a homogeneous laser beam profile at the cathode is favorable to achieve lowest electron emittance. Unfortunately effects linked to the frequency conversion process as well as beam propagation of the intense UV radiation to the cathode give rise to deterioration of the UV spatial profile. Shown in figure 8 is the UV beam profile at three locations in our laser beam path, such as at the THG crystal, at the hard aperture (used for producing a truncated Gaussian beam profile) and at the cathode. Efforts need to be undertaken to achieve the requested flattop transverse beam shape at the gun. The first version of our laser propagation path from the SFG crystal to the cathode consisted of free space propagation in air from the crystal to the aperture plane and imaging optics to image the truncated Gaussian on the cathode (Fig. 7a).

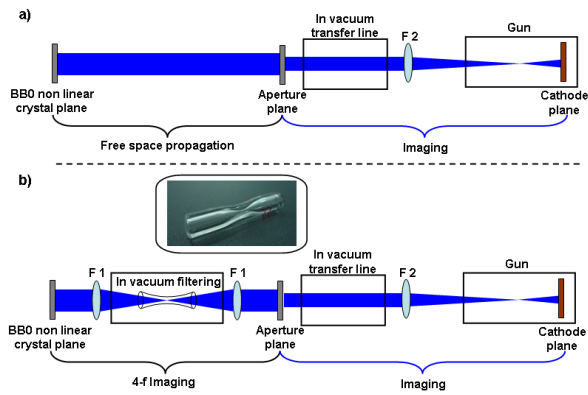


Figure 7: Schematic of the laser transfer line to the gun cathode. (a) old beam propagation setup without double imaging nor spatial filtering. (b) Improved setup with relay imaging and spatial filtering. The conceal capillary (inset) is made out of BK7 glass and has an inner diameter of 300 μm .

homogeneity, the beam profile was measured and analyzed by a home made algorithm (Matlab platform). The algorithm divides the beam into sections of equal areas and computes the normalized radial and angular root mean square (rms) intensity over the beam sections. It also plots these values as a function of the section number. Figure 8 summarizes the evolution of the transverse beam profile from the SFG crystal to the cathode. The beam profile after the SFG crystal exhibits several hotspots that are intrinsic to high-intensity frequency conversion with femtosecond pulses.

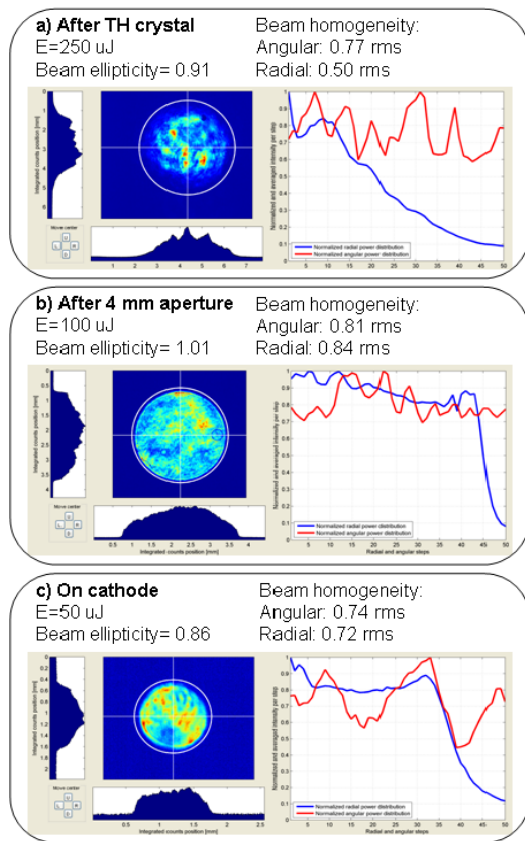


Figure 8: Measured transverse beam profile (left) and calculated normalized angular (blue) and radial (red) uniformity at various positions like (a) SFG crystal (b) aperture and (c) cathode position without spatial filtering.

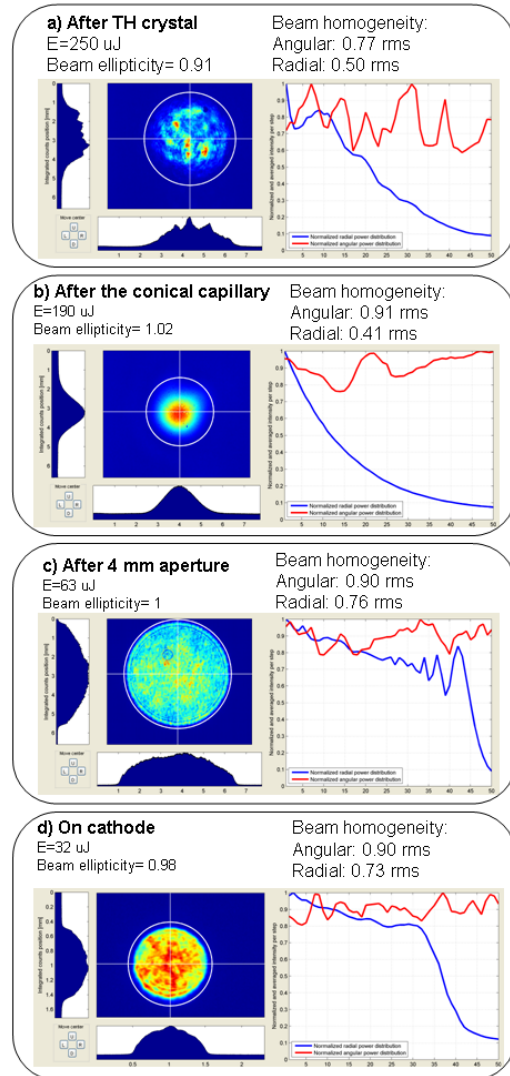


Figure 9: Measured transverse beam profile (left) and calculated normalized angular (blue) and radial (red) uniformity at the a) SFG crystal, b) after conical capillary, c) aperture and d) cathode position with conical capillary filtering.

At the aperture plane, the spatial clipping allows for better beam homogeneity at the expense of high energy losses (60%). At the cathode, however, the beam carries again a strong asymmetry and a rather poor angular and radial normalized homogeneity of 0.74 and 0.72 rms,

respectively. These transverse intensity patterns are not suitable for the generation of low emittance electron beams.

To improve the transverse beam profile various solutions were tested such as micro-lenses array or aspheric beam shaper but none of them was satisfying the requirements of our electron gun. We finally end up with the simple but reliable solution of Fourier filtering by help of a conical capillary. Standard metallic pinholes are not suitable for this application since they could be damaged by the high laser intensity and the sharp edge gives rise to strong unwanted diffraction rings. A smarter solution turns out to be a conical capillary set up in a 4-f imaging line under vacuum. The setup is depicted in figure 7b). Different to the previous setup the SFG crystal plane is imaged on the aperture plane. The imaging line is under vacuum and the conical capillary is placed at the intermediate focus (laser diameter 80 μm FWHM). Vacuum is mandatory to avoid spectral and temporal distortion induced by nonlinear effects in air. The conical capillary is made of BK7 and has an inner diameter of 300 μm . The diameter has been chosen in order to obtain a good trade-off of between beam transverse quality and energy throughput (typically 70-80%). Figure 9 shows the evolution of the beam transverse profile through the setup. After Fourier filtering in the capillary, the beam profile is very smooth and close to a TEM00 (Fig. 9b). The capillary throughput in the presented case is 76%. To obtain a flat top like transverse profile, spatial clipping by a 4 mm diameter aperture is still needed (Fig. 6c). However, the angular uniformity is significantly improved (red line) while the radial uniformity is comparable (blue line). The transverse beam quality enhancement is obvious on the cathode plane (Fig. 9d). The intensity profile is flat top like and the beam ellipticity is 0.98. Angular and radial normalized homogeneity are equal to 0.90 and 0.73 rms respectively. Finally, we measured the pulse energy and stability at various locations of the laser transfer line. The results are summarized in Table 1.

Table 1: Measured pulse energy and stability over 10 minutes (100% laser shots) at various locations of the laser transfer line (feedback systems off)

Location	Energy (μJ)	rms stability (%)	P-P Stability (%)
SFG crystal	250	0.9	5
Aperture	63	2.4	10.6
Cathode	32	2.5	11

The capillary introduced unwanted laser energy fluctuations. This came from a coupling between laser pointing and energy throughput by the capillary occurring whenever laser beam pointing drifts are present. In order to reduce this effect implementation of an active feedback on the laser position at the capillary plane was installed.

LASER-DRIVEN THZ SOURCE

The development of high-power single-cycle THz sources driven by lasers is motivated by various reasons. First, it seems favourable to produce THz radiation as close as

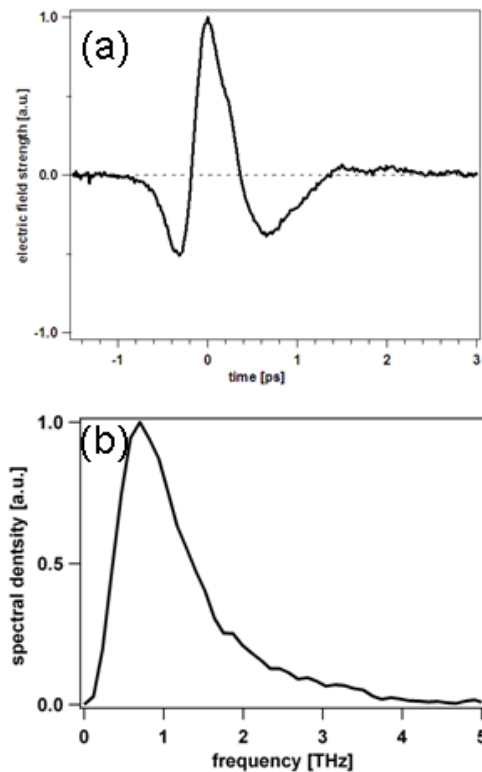


Figure 10: THz radiation in a laser-driven plasma with (a) electric field and (b) corresponding spectrum.

possible to the experimental area in order to reduce transport losses and to achieve best synchronization with a secondary laser (x-ray or optical). A THz source close to the experiment allows furthermore long and bulky THz beam transport systems, expensive in-vacuum propagation and large optics required due to the intrinsically large THz beam divergence. Our recent activities on laser-based THz source development focus on exploring table-top THz generation in plasma as well as in nonlinear optical crystals. Shown in figure 10 are preliminary results of THz pulses generated by an intense femtosecond laser pulses and its second harmonic. A nonlinear mixing process give rise to strong THz emission with field strength up to 400 kV/cm. The corresponding spectrum is centered around 1 THz. Many applications in science require, however, much higher field strength (up to several MV/cm) which seems hard to produce with plasma-based sources. Further investigations include therefore the study of THz formation in organic crystals.

CONCLUSION

We presented our latest developments on temporal and spatial laser beam shaping towards the future SwissFEL gun laser. A novel efficient frequency conversion scheme based on mixing oppositely chirped ps pulses in a thick crystal has been discussed and first results on flat-top temporal pulse shaping have been presented. Furthermore broadband amplification in Ti:sapphire amplifier has been investigated and the use of this technique for the realization of a wavelength tunable pulses in the infrared, deep UV and soft x-ray has been shown. Finally first

results on laser-based THz generation have been presented.

REFERENCES

- [1] A. M. Weiner, Rev. Sci. Instrum. 71, 1929 (2000)
- [2] A. Trisorio *et al.*, Opt. Express submitted (2011)
- [3] T. Oksenhendler *et al.*, Appl. Phys. B 83,p491 (2006)
- [4] A. Trisorio *e. al.*, CMC7, CLEO conference, Baltimore USA (2011)
- [5] K. Osvay *et al.*, J. Opt. Soc. Am. B 13,p1431 (1996)
- [6] C. Vicario *et al.* Opt. Lett. submitted (2011)